PERGAMON

Journal of the Mechanics and Physics of Solids
47 (1999) 971–992

JOURNAL OF THE
MECHANICS AND
PHYSICS OF SOLIDS

Hydrogen transport near a blunting crack tip

A.H.M. Krom[a,*], R.W.J. Koers[b], A. Bakker[a]

[a] *TNO Industrie, Laan van Westenenk 501, Postbus 541, 7300 AM Apeldoorn, The Netherlands*
[b] *Shell International Oil Products BV, Shell Research and Technology Centre, Badhuisweg 3, 1031 CM Amsterdam, The Netherlands*

Received 4 September 1997; in revised form 24 February 1998

Abstract

The hydrogen transport model of Sofronis and McMeeking was used in order to simulate the effect of the hydrostatic stress and trapping on the hydrogen distribution in a plastically deforming steel. In this model it is assumed that hydrogen atoms diffuse through lattice sites and that trap sites are filled by lattice diffusion. These trap sites are formed due to plastic deformations. Coupled diffusion elastic–plastic finite element analyses were carried out in order to investigate the hydrogen concentration in lattice and trap sites near a blunting crack tip under small-scale yielding conditions. The numerical results of Sofronis and McMeeking were reproduced and it was found that in their model hydrogen is created. The hydrogen balance is satisfied by including a strain rate factor in the hydrogen transport equation. As a consequence no differences were found at steady state, i.e. at low strain rates. The strain rate factor decreases the hydrogen concentration in lattice sites due to the filling of trap sites. When the strain rate is sufficiently high, the lattice sites can be almost depleted of hydrogen while trap sites remain saturated. The modified hydrogen transport model predicts strong dependence of the hydrogen concentration in lattice sites on the strain rate, while the hydrogen concentration in trap sites is not affected significantly. The modified hydrogen transport model provides greater insight into the strain rate dependence of hydrogen embrittlement as observed in tensile tests.

Keywords: Hydrogen trapping; Corrosion and embrittlement; A. Crack tip plasticity; A. Diffusion, bulk; C. Finite elements

1. Introduction

The mechanism of hydrogen embrittlement is still not clear, despite many years of intensive investigation. Over the years a number of theories have been developed, of

* Corresponding author. E-mail: a.krom@ind.tno.nl

0022–5096/99/$ - see front matter
PII: S0022–5096(98)00064–7

which the most important are (Turnbull, 1993) : the hydrogen phase change theory, the pressure theory, the decohesion theory and the hydrogen enhanced local plasticity (HELP) theory. The overall opinion is that no single mechanism is applicable to all metals plus environments. Hydrogen embrittlement generally requires localization of hydrogen atoms, which can occur at trap sites such as dislocations, grain boundaries, interfaces between different phases, voids or cracks. Kumnick and Johnson (1980) carried out permeation tests on iron deformed to different amounts of plastic strain. These tests show that hydrogen trapping depends on the amount of plastic strain. Localization of hydrogen can also occur through the effect of hydrostatic stress on the chemical potential. Sun et al. (1995) investigated the hydrogen distribution around a crack tip in an fcc single crystal. Their results show that there are two peaks of hydrogen concentration ahead of the crack tip : one peak is in the immediate vicinity of the crack tip, corresponding to the location of maximum equivalent strain, and another peak is located at some distance from the crack tip, corresponding to the location of the maximum hydrostatic stress. These two peaks in the hydrogen distribution were also found by Gao et al. (1994) in a low-alloy steel. Hydrogen embrittlement is also strain rate dependent, as shown by tensile tests. These tests show a decreasing strain at fracture with decreasing loading rate, see for example Maier et al. (1995). In order to model the effects of the hydrostatic stress and hydrogen trapping due to plasticity on the hydrogen distribution in a body, a coupled diffusion elastic–plastic stress analysis is necessary. The finite element method is a very useful tool for this purpose. To the knowledge of the authors, Sofronis and McMeeking (1989) are the only researchers who have so far carried out coupled diffusion elastic–plastic stress finite element analyses incorporating the effect of hydrostatic stress and trapping. Toribio et al. (1995) also carried out coupled finite element analyses on notched bars but without the trapping of hydrogen.

In this paper the hydrogen transport model of Sofronis and McMeeking (1989) is used. It will be shown that the original hydrogen transport model does not provide a correct hydrogen balance. A modification is proposed which includes a factor depending on the strain rate. The modified hydrogen transport model provides a correct hydrogen balance. In addition the effect of the strain rate factor on the hydrogen concentrations near a blunting crack tip will be demonstrated. The effect of strain rate will also be investigated. Finally, the significance of the modified hydrogen transport model will be discussed in relation to hydrogen embrittlement as observed in tensile tests.

2. Hydrogen transport equation

We follow the hydrogen transport model of Sofronis and McMeeking (1989), which is based on the equilibrium theory presented by Oriani (1970) and Johnson and Lin (1981). Note that the subscript L refers to lattice sites and the subscript T to trap sites. It is assumed that traps are isolated, i.e. do not form an extended network. Hence, hydrogen transport between trap sites is by lattice diffusion. Moreover, we consider only one kind of trap, i.e. one which is saturable and reversible, such as a

dislocation core. Considering a body with volume V and surface S, mass conservation requires that the rate of change of total hydrogen inside V is equal to the flux through S:

$$\frac{\partial}{\partial t}\int_V \{C_L + C_T\}\,\mathrm{d}V + \int_S \mathbf{J}\cdot\mathbf{n}\,\mathrm{d}S = 0, \tag{1}$$

where $\partial/\partial t$ is the partial derivative with respect to time, C_L is the hydrogen concentration in lattice sites, C_T is the hydrogen concentration in trap sites, $\mathbf{n}$ is the outward-pointing unit normal vector and $\mathbf{J}$ the hydrogen flux, defined as

$$\mathbf{J} = -M_L C_L \nabla\mu_L, \tag{2}$$

where M_L is the mobility of the hydrogen in lattice sites and μ_L the chemical potential of the hydrogen in the lattice sites. There is no direct evidence available indicating which type of interstitial site is occupied by the hydrogen atom in α-iron. Whether hydrogen atoms occupy tetrahedral or octahedral sites in α-iron, both sites are too small for the hydrogen atom. Hence, the dissolved hydrogen atom causes a volume increase in α-iron. The chemical potential of hydrogen in regions of a tensile hydrostatic stress is therefore lower. As a consequence, a hydrogen flux is generated towards these regions in order to lower the chemical potential. The opposite effect occurs of course in the regions of compressive hydrostatic stresses. The chemical potential of hydrogen in lattice sites in a body under stress, neglecting higher-order terms of the hydrostatic stress σ_h (first-order approach), is

$$\mu_L = \mu_L^0 + RT\ln\frac{C_L}{N_L} - \bar{V}_H\sigma_h, \tag{3}$$

where μ_L^0 is the chemical potential at a reference temperature and pressure, $\bar{V}_H$ the partial molar volume of hydrogen, i.e. $2.0\times10^{-6}\,\mathrm{m}^3$ for α-iron at 293 K (Hirth, 1980), σ_h the hydrostatic stress: $\sigma_h = \frac{1}{3}\Sigma_{i=1}^{3}\sigma_{ii}$. Subsitution of (3) in (2) results in

$$\mathbf{J} = -D_L\nabla C_L + \frac{D_L C_L \bar{V}_H}{RT}\nabla\sigma_h, \tag{4}$$

where D_K is the concentration independent lattice diffusivity: $D_L = M_L RT$. Substitution of (4) in (1) gives

$$\int_V \left\{\frac{\partial C_L}{\partial t} + \frac{\partial C_T}{\partial t}\right\}\mathrm{d}V + \int_S \left\{\left(-D_L\nabla C_L + \frac{D_L C_L \bar{V}_H}{RT}\nabla\sigma_h\right)\cdot\mathbf{n}\right\}\mathrm{d}S = 0). \tag{5}$$

Using the divergence theorem we find

$$\int_V \left\{\frac{\partial C_L}{\partial t} + \frac{\partial C_T}{\partial t} - \nabla\cdot(D_L\nabla C_L) + \nabla\cdot\left(\frac{D_L C_L \bar{V}_H}{RT}\nabla\sigma_h\right)\right\}\mathrm{d}V = 0. \tag{6}$$

Since this equation holds for an arbitrary volume V, the integrand must vanish, or:

$$\frac{\partial C_L}{\partial t} + \frac{\partial C_T}{\partial t} - \nabla\cdot(D_L\nabla C_L) + \nabla\cdot\left(\frac{D_L C_L \bar{V}_H}{RT}\nabla\sigma_h\right) = 0. \tag{7}$$

A relation for the partial derivative of the hydrogen concentration in trap sites with respect to time will be derived. The hydrogen concentrations are first related to the number of sites:

$$C_L = \theta_L N_L, \tag{8}$$

where θ_L is the occupancy of lattice sites and N_L the number of lattice sites per unit volume, and

$$C_T = \theta_T N_T, \tag{9}$$

where θ_T is the occupancy of the trap sites and N_T the trap density, i.e. the number of trap sites per unit volume. Oriani (1970) and Johnson and Lin (1980) give an expression for the hydrogen concentration in trap sites as a function of the hydrogen concentration in lattice sites in the case of equilibrium

$$C_T = \frac{N_T}{1 + \dfrac{1}{K_T \theta_L}}, \tag{10}$$

where K_T is the trap equilibrium constant: $K_T = e^{-\Delta E_T/RT}$ with ΔE_T the trap binding energy with respect to the lattice site, R the universal gas constant, i.e. 8.3144 J/mol/K and T the absolute temperature. As shown by Kumnick and Johnson (1980), the number of trap sites depends on the deformation level. Hence,the number of trap sites can be expressed as a function of equivalent plastic strain ε_p. Since the number of lattice sites is a constant and the temperature will be kept constant, the partial derivative of the hydrogen concentration in trap sites with respect to time becomes

$$\frac{\partial C_T}{\partial t} = \frac{\partial C_T}{\partial C_L}\frac{\partial C_L}{\partial t} + \frac{\partial C_T}{\partial N_T}\frac{dN_T}{d\varepsilon_p}\frac{\partial \varepsilon_p}{\partial t}. \tag{11}$$

The partial derivative of the hydrogen concentration in trap sites with respect to the hydrogen concentration in lattice sites, using (10), is

$$\frac{\partial C_T}{\partial C_L} = \frac{C_T(1-\theta_T)}{C_L}. \tag{12}$$

The partial derivative of the hydrogen concentration in trap sites with respect to the number of trap sites, using (9) is

$$\frac{\partial C_T}{\partial N_T} = \theta_T. \tag{13}$$

Substituting (12) and (13) in (11), the partial derivative of the hydrogen concentration in trap sites with respect to time is

$$\frac{\partial C_T}{\partial t} = \frac{C_T(1-\theta_T)}{C_L}\frac{\partial C_L}{\partial t} + \theta_T \frac{dN_T}{d\varepsilon_p}\frac{\partial \varepsilon_p}{\partial t}. \tag{14}$$

Finally, using (14), (7) becomes

$$\frac{C_L + C_T(1-\theta_T)}{C_L}\frac{\partial C_L}{\partial t} - \nabla\cdot(D_L\nabla C_L) + \nabla\cdot\left(\frac{D_L C_L \bar{V}_H}{RT}\nabla\sigma_h\right) + \theta_T\frac{dN_T}{d\varepsilon_p}\frac{\partial\varepsilon_p}{\partial t} = 0. \tag{15}$$

The last term in (15) is called the (plastic) strain rate factor. This was not taken into account in the model of Sofronis and McMeeking (1989). The variational and finite element form of (15) can be found in the Appendix.

The trap density and derivative $dN_T/d\varepsilon_p$ can be obtained from the data of Kumnick and Johnson (1980), who carried out permeation tests on pure iron with hydrogen gas charging and found that the trap density in iron increases sharply with deformations at low deformation levels and then increases more gradually with further deformation. They also estimated a trap binding energy of -60 kJ/mol, independent of deformation level within the range of 0–80% cold work and independent of temperature within the range of 288–343 K, suggesting one type of trap. A fit of the number of trap sites vs equivalent true plastic strain which is close to their experimental observations and to the fit used by Sofronis and McMeeking (1989) is

$$\log N_T = 23.26 - 2.33\,e^{-5.5\varepsilon_p}. \tag{16}$$

The number of lattice sites N_L is related to the properties of the metal atom:

$$N_L = \frac{N_A\beta\rho}{A_r}, \tag{17}$$

with β the number of interstitial lattice sites per metal atom, N_A Avogadro's number, i.e. 6.022×10^{23} mol^{-1}, ρ the density of the metal, i.e. 7.87×10^3 kg/m^3 for iron at 293 K (*Smithells Metals Reference Book*, 1992), and A_r the atomic weight, i.e. 55.8×10^{-3} kg/mol for iron at 293 K (*Smithells Metals Reference Book*, 1992). Indirect evidence indicates tetrahedral site occupancy rather than octahedral site occupancy at room temperature in α-iron (Hirth, 1980; Kiuchi and McLellan, 1983) in which case β is 6. Hence (17) gives: $N_L = 5.1\times10^{29}$ m^{-3}.

3. The effect of the strain rate factor in the case of an insulated, uniformly-stressed body

In order to demonstrate the effect of the strain rate factor, we consider a volume element in an insulated plastically deforming body which is uniformly-stressed and has a uniform starting hydrogen concentration. This is a problem without hydrogen diffusion. Firstly, the gradients of the hydrostatic stress are zero, since the body is uniformly stressed. Secondly, the total hydrogen concentration, $C_{tot} = C_L + C_T$, must remain constant during the loading history, since the body is insulated. Hence, there is only a redistribution of hydrogen between lattice and trap sites. In this case the solution of (15) results in (10) which can now be rewritten as

$$C_T^2 - \left(\frac{N_L}{K_T} + C_{tot} + N_T\right)C_T + N_T C_{tot} = 0. \tag{18}$$

This quadratic equation of the hydrogen concentration in trap sites has one correct solution, given by

$$C_T = \frac{1}{2}\left\{\frac{N_L}{K_T} + C_{tot} + N_T - \sqrt{\left(\frac{N_L}{K_T} + C_{tot} + N_T\right)^2 - 4N_T C_{tot}}\right\}. \tag{19}$$

The other solution is not valid, as it results in a negative hydrogen concentration in lattice sites. Using (19) together with (16), the hydrogen concentration in lattice and trap sites as a function of equivalent plastic strain is shown in Fig. 1. The hydrogen concentration in trap sites increases with increasing plastic strain, while the hydrogen concentration in lattice sites decreases down to 0.2 plastic strain. While the number of trap sites is still increasing, these sites are no longer filled due to the fact that the lattice sites are almost empty. Since there is equilibrium between the hydrogen in lattice sites and the hydrogen in trap sites, the hydrogen concentration in lattice sites cannot become zero. Also shown in Fig. 1 are the finite element results of one element calculations based on the hydrogen transport model and on the modified hydrogen

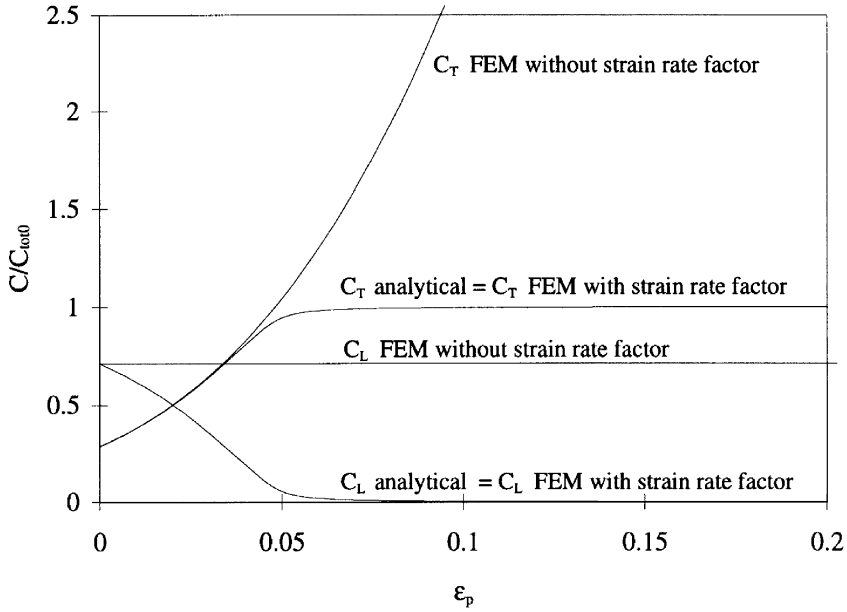

Fig. 1. Hydrogen concentration in lattice and trap sites as a function of equivalent plastic strain in an insulated, uniformly-stressed body according to the analytical solution (19), the FEM result of the hydrogen transport model of Sofronis and McMeeking and the FEM result of the modified hydrogen transport model. C_{tot0} is the total hydrogen concentration at $\varepsilon_p = 0$. At $\varepsilon_p = 0$, $C_L = 2.08 \cdot 10^{21}$ m^{-3} and $C_T = 8.42 \cdot 10^{20}$ m^{-3}.

transport model. In the case of the hydrogen transport model the hydrogen concentration in lattice sites remains constant, while the hydrogen concentration in trap sites increases until the number of trap sites becomes constant. At 0.8 plastic strain, the total hydrogen concentration is 60 times greater than the initial total hydrogen concentration. Since the body is insulated, this means that hydrogen is created. In the case of the modified hydrogen transport model, i.e. with the strain rate factor, the finite element result coincides with the analytical solutions, i.e. (19). Thus the modified hydrogen transport model provides a correct hydrogen balance.

4. Hydrogen distribution near a blunting crack tip

4.1. *Mesh, boundary conditions and material properties*

The boundary layer approach is used in order to investigate the hydrogen distribution around a blunting crack tip without having to model a complete geometry. Sufficiently close to the crack tip, stresses and strains are controlled by the mode I stress intensity factor K_I. The approach is valid as long as small-scale yielding conditions hold. Due to symmetry, it is only necessary to model a semi-circular region $0 \leqslant \theta \leqslant \pi$ relative to the crack tip. The mesh used is approximately the same as the one used by Sofronis and McMeeking (1989). It consists of 960 four-node, plane strain elements: 40 elements in the radial direction and 24 elements in the tangential direction. The elements increase in size in the radial direction by a growth factor of 1.29. The only length parameter is the initial crack tip opening displacement b_0 (twice the initial crack radius) which is 10 μm. The radius of the semi-circular mesh is 15,000 b_0. On the symmetry axis the hydrogen flux is zero while on the circular boundary and the crack surface the hydrogen concentration in lattice sites is prescribed, i.e. the initial hydrogen concentration in lattice sites C_{L0}. On the symmetry axis the displacements in the y direction are zero, while on the circular boundary the displacements are known from the elastic solution, which is controlled by K_I. The crack surface is stress-free. In each increment a diffusion analysis is carried out followed by an updated Lagrangian stress analysis. The diffusion coefficient D_L at 300 K is $1.27 \times 10^{-8}\,\mathrm{m^2/s}$ and the initial hydrogen concentration in lattice sites C_{L0} is $2.08 \times 10^{21}\,\mathrm{m^{-3}}$, corresponding to hydrogen gas of 1 atm at 300 K (Sofronis and McMeeking, 1989). The uniaxial stress–strain relation is given in the form of a power law

$$\varepsilon = \begin{cases} \dfrac{\sigma}{E} & \text{if } \varepsilon \leqslant \dfrac{\sigma_y}{E} \\ \dfrac{\sigma_y}{E}\left(\dfrac{\sigma}{\sigma_y}\right)^n & \text{if } \varepsilon > \dfrac{\sigma_y}{E} \end{cases},$$

where E is Young's modulus, i.e. 207 GPa, σ_y is the yield stress, i.e. 250 MPa, and n the hardening exponent, i.e. 5. Poisson's constant is 0.3. A maximum load of $K_I = 89.2$ MPa$\sqrt{\mathrm{m}}$ is reached in a period of 130 s with steps of 0.5 s. At 130 s the crack tip

opening displacement b, according to 45° intercept definition of Tracey (1976), was 4.7 times the initial crack tip opening displacement b_0. After 130 s the load was kept constant and the time step was increased to 5 s up to 835 s and then increased again to 100 s up to 1419 h.

4.2. *Results of calculations on the boundary layer*

We first consider the hydrogen transport model of Sofronis and McMeeking. The results are compared with the results of Sofronis and McMeeking (1989), which are taken from Fig. 6 of their paper. In Fig. 2 the hydrostatic stress ahead of the crack tip in the ligament ($\theta = 0°$) is given after 130 s, i.e. the end of loading time. There is a slight difference in the height of the peak, probably caused by differences in the meshes and/or in the stress–strain relation, which was given in Kirchhoff stresses while our finite element program uses the stress–strain relation in Cauchy stresses. Nevertheless, the result matches those of Sofronis and McMeeking very well. Next, we compared the hydrogen distribution in lattice sites at 130 s and at 1419 h (5.1×10^6 s), see Fig. 3. Again, the results match very well. The differences are caused by the difference in the hydrostatic stress distribution as shown in Fig. 2. The result for the hydrogen concentration in trap sites also matches rather well (not shown). We can therefore conclude that the finite element implementation of the hydrogen transport model of Sofronis and McMeeking (1989) is correct.

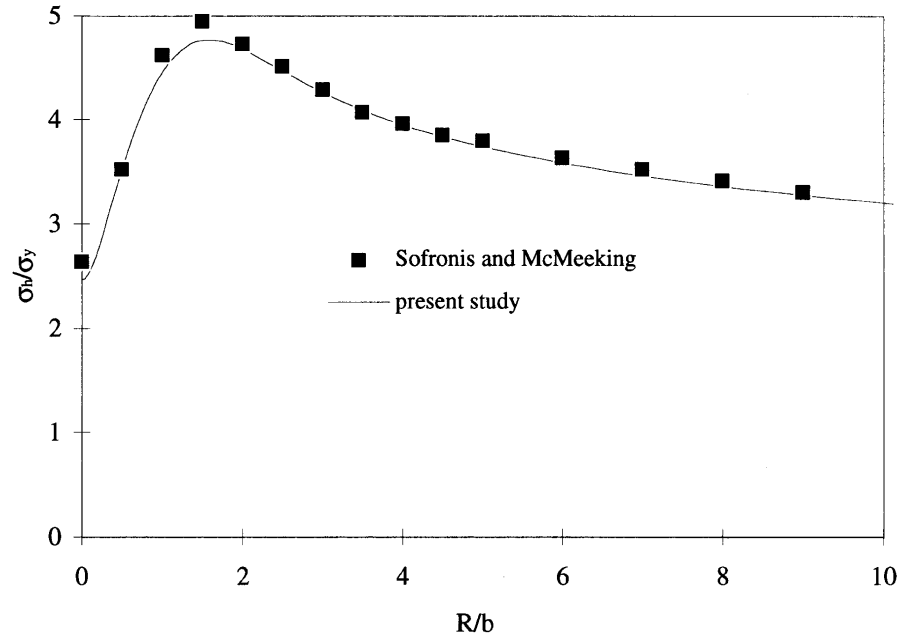

Fig. 2. The hydrostatic stress ahead of the crack tip ($\theta = 0°$) at 130 s (end of loading) compared with the result of Sofronis and McMeeking (1989). σ_y is the yield stress and b the crack tip opening displacement.

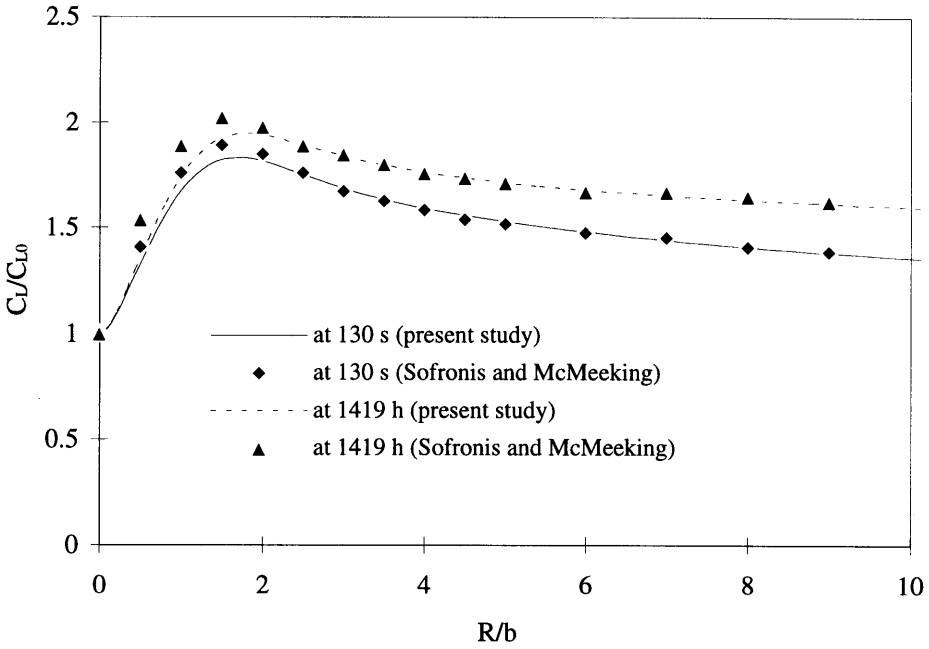

Fig. 3. The hydrogen concentration in lattice sites ahead of the crack tip ($\theta = 0°$) at 130 s (end of loading) and at 1419 h according to the hydrogen transport model of Sofronis and McMeeking (1989), compared with the results of Sofronis and McMeeking (1989). C_{L0} is the initial hydrogen concentration in lattice sites and b the crack tip opening displacement.

Secondly, we consider the modified hydrogen transport model. The effect of the strain rate factor on the hydrogen distribution in lattice sites is shown in Fig. 4. For comparison purposes the results without the strain rate factor are also shown. At 130 s the hydrogen distribution in lattice sites with the strain rate factor is lower than without the strain rate factor. This is in agreement with the results of the previous section. At 1419 h the hydrogen distributions of both transport models coincide. Apparently steady state is reached within 1419 h and rate effects are no longer present. In order to investigate the steady-state situation further we consider the hydrogen concentration in lattice and trap sites at the location of maximum hydrostatic stress. In Fig. 5 the hydrogen concentrations at the location of maximum hydrostatic stress at 130 s are shown as a function of time. Till 130 s both hydrogen concentrations increase. After 130 s the hydrogen concentration in trap sites remains constant, since trap sites are no longer created and saturation of trap sites is reached. The hydrogen concentration in lattice sites is still increasing but at a decreasing rate up to a certain limit. It can be concluded that a steady-state situation is reached after approximately 10^4 s ($\approx$3 h), i.e. long before 1419 h.

Compared with the previous section the effect of the strain rate factor is not large because in this section the hydrogen concentration in lattice sites is prescribed on the boundaries. As a consequence the lattice sites can be filled with hydrogen again, thus

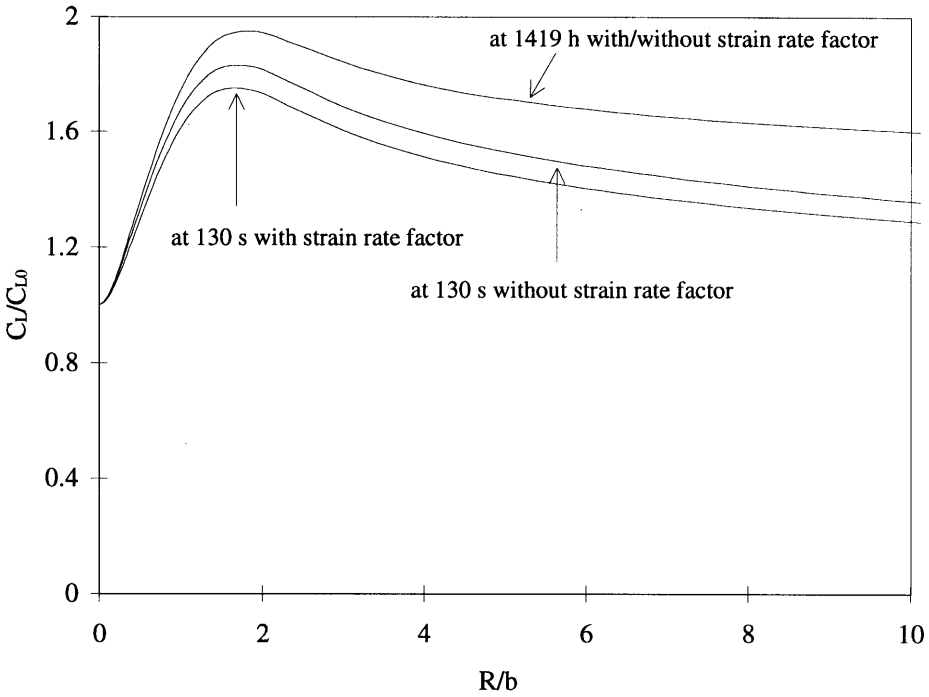

Fig. 4. The hydrogen concentration in lattice sites ahead of the crack tip ($\theta = 0°$) at 130 s (end of loading) and at 1419 h, showing the effect of the strain rate factor in the hydrogen transport equation. C_{L0} is the initial hydrogen concentration in lattice sites and b the crack tip opening displacement.

diminishing the strain rate effect. The effect of the strain rate factor becomes more pronounced when the strain rate is increased. This will be discussed in the next section.

5. Effect of strain rate on hydrogen distributions near a blunting crack tip

The effect of strain rate is investigated by changing the loading time to reach a load of $K_I = 89.2$ MPa$\sqrt{}$m. Thus, the longer the loading time, the lower the strain rate. The material parameters are assumed to be strain rate independent. First we discuss the case in which the boundaries, i.e. the circular boundary and the crack surface, have a prescribed hydrogen concentration equal to C_{L0}. In Fig. 6 the hydrogen concentration in lattice sites at the end of loading along the symmetry axis is shown for different loading times. At a loading time of 1.3 s, the strain rate is so high that the diffusion of hydrogen cannot deliver the hydrogen for the lattice sites which are depleted of hydrogen due to trapping. At the crack tip there is a small region with high plastic strains and thus with a high number of trap sites which are filled due to the high trap binding energy. The hydrogen for the trap sites is supplied from the hydrogen in lattice sites. Hence the hydrogen concentration in lattice sites becomes

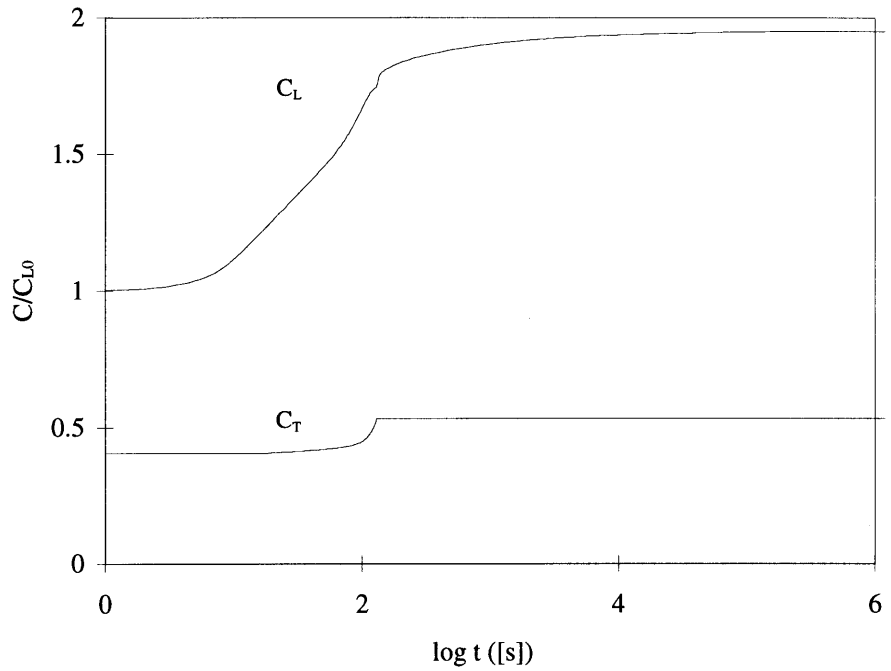

Fig. 5. The hydrogen concentration in lattice and trap sites at the location of the maximum hydrostatic stress, as a function of time. The load was kept constant at 130 s. The hydrogen concentration is prescribed on the crack surface. C_{L0} is the initial hydrogen concentration in lattice sites.

lower than the initial hydrogen concentration. Since the hydrogen concentration on the crack surface is prescribed, the hydrogen concentration in lattice sites rises again to the surface. With increasing loading time, the time for hydrogen diffusion increases,the depleted lattice sites can be filled again and the peak due to the hydrostatic stress appears. Increasing the loading time to more than 1.3×10^6 s does not give a higher hydrogen distribution. At a loading time of 1.3×10^6 s the lattice sites which are depleted by trapping are directly filled again by hydrogen diffusion. As a consequence this hydrogen distribution must coincide with the steady-state solution. In the previous section it was shown that the steady-state distribution is reached long before 1419 h. The hydrogen distribution after a loading time of 1.3×10^6 s indeed coincides with the hydrogen distribution at 1419 h after a loading time of 130 s.

The hydrogen concentration in trap sites, see Fig. 7, shows a high peak at the crack tip of about 86 times the initial hydrogen concentration in lattice sites. The strain rate has little effect on the peak within the loading times investigated as the trap binding energy is very high. The trapping of hydrogen is necessary, however, for the strain rate dependence. Without this the strain rate has only a slight effect on the hydrogen distribution in lattice sites.

We next discuss the case in which the boundaries, i.e. the circular boundary and the crack surface, are insulated. As a result of the insulation there is no supply of

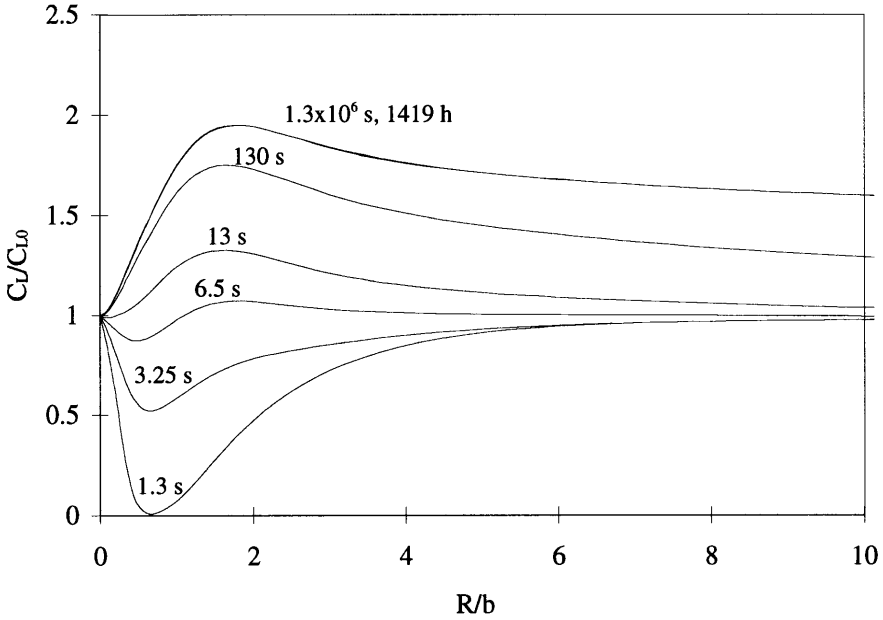

Fig. 6. The hydrogen concentration in lattice sites ahead of the crack tip after loading to $K_I = 89.2$ MPa$\sqrt{m}$ for different loading times. The result at 1419 h for a loading time of 130 s is also shown. The hydrogen concentration is prescribed on the crack surface. C_{L0} is the initial hydrogen concentration in lattice sites and b the crack tip opening displacement.

hydrogen through the boundaries and the total hydrogen content in the boundary layer remains constant. In Fig. 8 the hydrogen concentration in lattice sites at the end of loading along the symmetry axis is shown for different loading times. Again at a loading time of 1.3 s, the strain rate is so high that the diffusion of hydrogen cannot deliver the hydrogen for the lattice sites which are depleted by trapping. Due to the insulated crack surface the lattice sites at the crack tip are also depleted of hydrogen. With increasing loading time, the time for hydrogen diffusion increases, the depleted lattice sites can be filled again and the peak due to the hydrostatic stress appears. However, the filling of lattice sites is now slower, since the hydrogen must be supplied from the bulk. Again, increasing the loading time to more than 1.3×10^6 s does not give a higher hydrogen distribution. At a loading time of 1.3×10^6 s the lattice sites which are depleted by trapping are directly filled again by hydrogen diffusion. As a consequence this hydrogen distribution must coincide with the steady-state hydrogen distribution which is reached before 1419 h. Indeed, the hydrogen distribution coincides with the hydrogen distribution at 1419 h after a loading time of 130 s. The steady-state hydrogen distribution is now higher, since the insulated crack surface does not take away hydrogen.

The hydrogen distribution in trap sites again shows a high peak at the crack tip, see Fig. 9. The height of this peak is about 86 times the initial hydrogen concentration

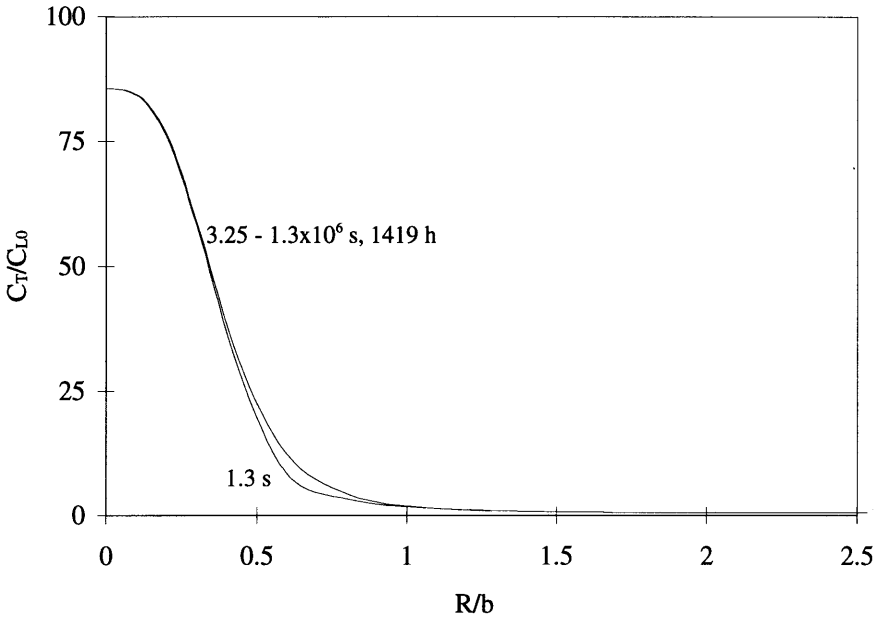

Fig. 7. The hydrogen concentration in trap sites straight ahead of the crack tip after loading to $K_I = 89.2$ MPa$\sqrt{m}$ for different loading times. The result at 1419 h for a loading time of 130 s is also shown. The hydrogen concentration is prescribed on the crack surface. C_{L0} is the initial hydrogen concentration in lattice sites and b the crack tip opening displacement.

in lattice sites. Only when the loading time is 1.3 s, the height reduces to 38 C_{L0}. This is a result of the assumption of equilibrium between hydrogen in lattice sites and trap sites, which is still valid despite the high strain rates (Krom, 1998). Near the crack the hydrogen concentration in lattice sites is extremely low compared with the initial hydrogen concentration in lattice sites. As a result, the hydrogen concentration in trap sites is somewhat lower than at longer loading times. Compared with the hydrogen distribution in lattice sites, however, the effect of the strain rate on the hydrogen concentration in trap sites is still slight.

6. Discussion of results

The results contained in the previous sections show that given the material parameters the strain rate has a considerable influence on the hydrogen concentration in lattice sites as a result of the creation of traps sites, i.e. trap sites created during plastic deformations. The effect of the traps depends on the temperature, the trap binding energy, the number of trap sites and the initial hydrogen concentration in lattice sites. These parameters are related by (10). Increasing the parameters which increase the hydrogen concentration in trap sites will result in a greater effect of the strain rate on

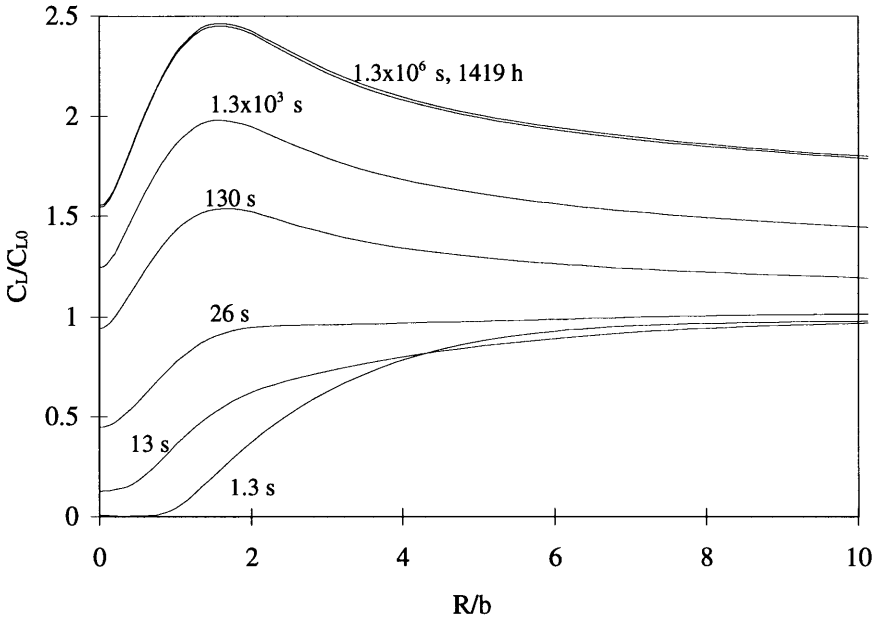

Fig. 8. The hydrogen concentration in lattice sites straight ahead of the crack tip after loading to $K_I = 89.2$ MPa$\sqrt{m}$ for different loading times. The result at 1419 h for a loading time of 130 s is also shown. The crack surface is insulated. C_{L0} is the initial hydrogen concentration in lattice sites and b the crack tip opening displacement.

the hydrogen concentration in lattice sites. Considering the total hydrogen distribution two peaks can be found: the highest one is found at the crack tip and is approximately 86 times the initial hydrogen concentration in lattice sites and corresponds to the peak in the plastic strain distribution. The height of this peak depends on the number of trap sites. The other peak can be found some distance away from the crack tip: it corresponds to the location of maximum hydrostatic stress. The height of this peak depends on the temperature and the yield stress. In the investigations on which this paper is based the yield stress was relatively low, i.e. 250 MPa. Increasing the initial hydrogen concentration will decrease the relative amount of hydrogen moved to trap sites. Hence the effect of the strain rate on the hydrogen distribution in lattice sites will become less as the hydrogen concentration in lattice sites increases. Ultimately the strain rate will have no effect. On the other hand increasing the number of trap sites due to plastic strains will result in a greater effect of the strain rate. Opposite effects will occur when these parameters decrease.

In the calculations two types of boundary conditions were considered: prescribed hydrogen concentration on the crack surface and insulated crack surface. The outer surface, i.e. the radius of the boundary layer, is so far away from the crack tip that it has no influence on processes at the crack tip. In practice these two boundary conditions can be seen as two extremes: when the surface reactions are slow compared

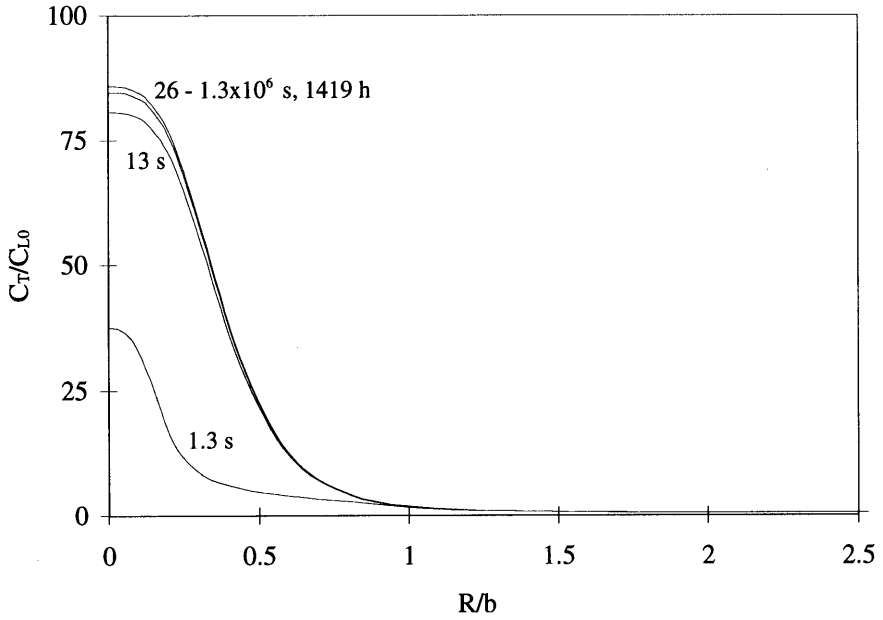

Fig. 9. The hydrogen concentration in trap sites straight ahead of the crack tip after loading to $K_I = 89.2$ MPa$\sqrt{m}$ for different loading times. The result at 1419 h for a loading time of 130 s is also shown. The crack surface is insulated. C_{L0} is the initial hydrogen concentration in lattice sites and b the crack tip opening displacement.

with the hydrogen lattice diffusion, the crack surface can be regarded as insulated. When the surface reactions are fast compared with the hydrogen lattice diffusion, the crack surface can be regarded as a surface with a prescribed hydrogen concentration. When the crack surface is insulated, the effect of strain rate is greater as the hydrogen must be supplied from the lattice around the plastic zone. Thus, the diffusion distance is greater. Moreover, the peak in the hydrogen distribution due to hydrostatic stress is higher when the crack surface is insulated. Nevertheless, the conclusions drawn from the results of both boundary conditions are the same.

Not only the level of the hydrogen concentrations is important but also the size and form of the region in which the hydrogen concentrations are changed, see Figs 10 and 11. The region of high hydrogen concentration in trap sites, situated at the blunting crack surface, is very small compared with the region in which the hydrogen concentration in lattice sites changes. The region of high hydrogen concentration in trap sites is almost independent of the strain rate and the type of boundary condition. The hydrogen distribution in lattice sites gradually transforms as the strain decreases. At high strain rates a region with the same form as the plastic zone develops, in which the hydrogen concentration in lattice sites is very low. At low strain rates a region develops which has the same form as the hydrostatic stress distribution. With the exception of the region close to the blunting crack tip surface, the boundary conditions do not have any great influence on the hydrogen distributions.

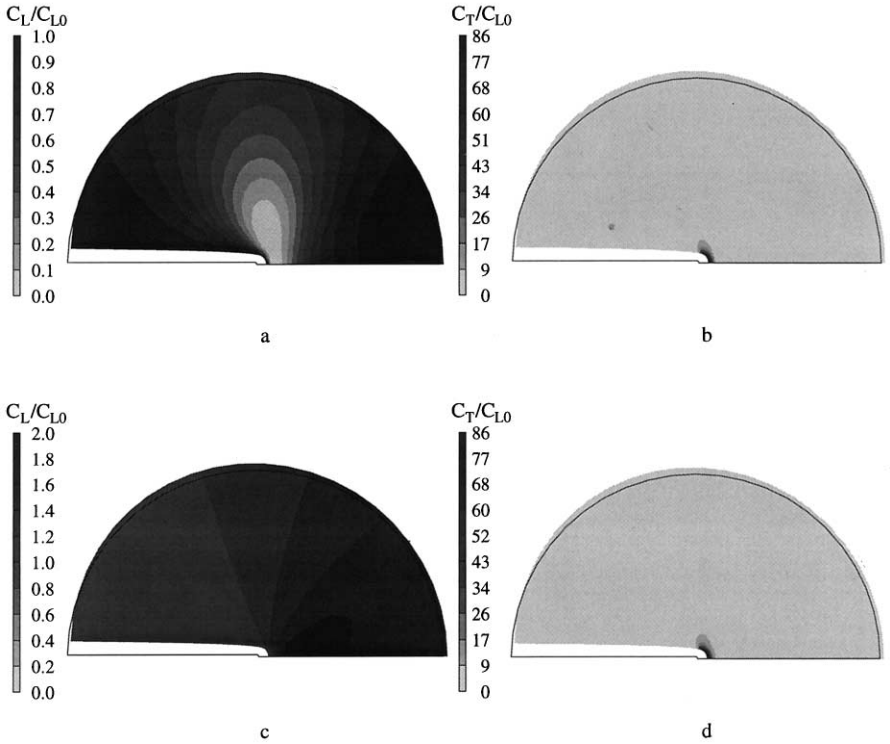

Fig. 10. Hydrogen distribution in the case of a constant surface concentration (detail at the crack tip, solid line indicates the undeformed mesh): (a) in lattice sites for a loading time of 1.3 s; (b) in trap sites for a loading time of 1.3 s; (c) in lattice sites for a loading time of 1.3×10^6 s; (d) in trap sites for a loading time of 1.3×10^6 s.

7. Implications for hydrogen embrittlement in tensile tests

Although the stress field and dislocation distributions in tensile specimens are different from those around crack tips, the mechanistic insights gained from modelling near-crack-tip regions can be applied usefully to the behavior of tensile specimens. Maier et al. (1995) carried out tensile tests in which low-alloy steel specimens were cathodically charged and elongated with different strain rates. The charging current density was so low that no damage was found from the loading itself. Moreover, the slope of the stress–strain curve and the ultimate tensile strength were not affected. There was, however, a marked reduction in the ductility, depending on the charging current density and the strain rate. When the strain rate was sufficiently high the fracture elongation was the same as in air. With decreasing strain rate the fracture elongation decreased while the fracture mechanism, void initiation, growth and coalescence, did not change. In addition, the fracture elongation decreased as the charging

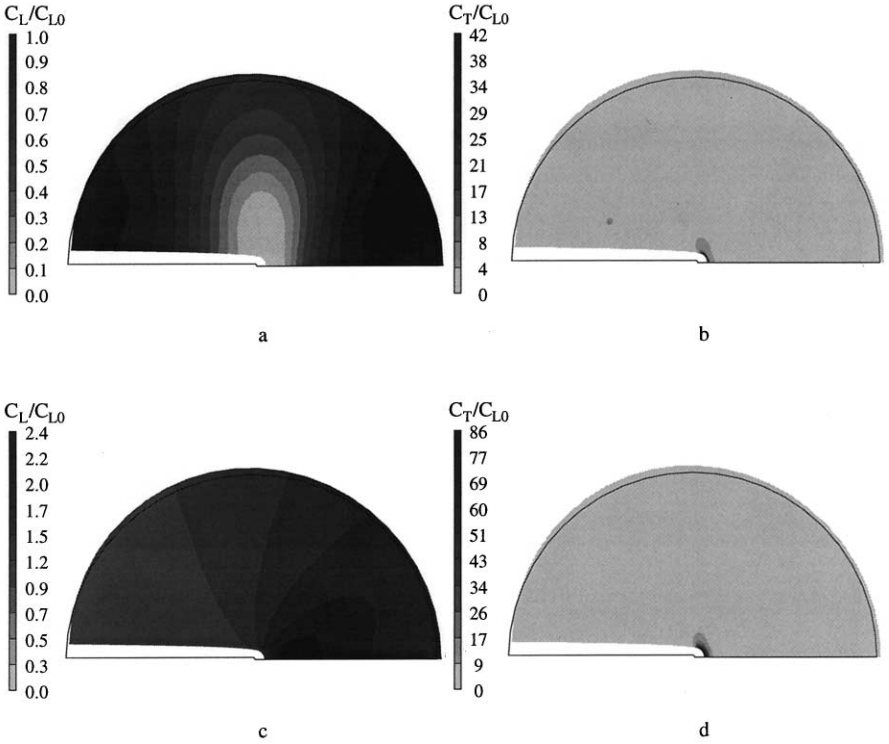

Fig. 11. Hydrogen distribution in the case of insulated surfaces (detail at the crack tip, solid line indicates the undeformed mesh) : (a) in lattice sites for a loading time of 1.3 s ; (b) in trap sites for a loading time of 1.3 s ; (c) in lattice sites for a loading time of 1.3×10^6 s ; (d) in trap sites for a loading time of 1.3×10^6 s.

current density increased. Similar results are reported by Garber et al. (1981) for spheroidized carbon steel and by Cialone and Asaro (1981) for spheroidized plain carbon steels.

These experimental results could well be explained by the modified hydrogen transport model. Firstly as shown by the present numerical results, the hydrogen concentration in trap sites is fairly independent of strain rate owing to the high binding energy. It is then quite reasonable to assume that trapped hydrogen does not contribute to the embrittlement mechanism. This means that we must consider not the total amount of hydrogen but only the hydrogen in lattice sites. When the strain rate is sufficiently high, the hydrogen concentration in lattice sites is much lower than the initial hydrogen concentration. This situation could correspond to the situation in which the same fracture elongation is obtained as in air. As the strain rate decreases, the hydrogen concentration in lattice sites increases up to a steady-state value which depends on the hydrostatic stress and the boundary conditions. This situation could correspond to the situation in which the minimum fracture elongation is obtained. When the initial hydrogen is increased, the effect of the strain rate on the depletion

of lattice sites will decrease, as there is more hydrogen available. This situation could correspond to the effect of the increasing charging current on the fracture elongation.

8. Conclusions

Coupled diffusion elastic–plastic finite element analyses were carried out in order to investigate the hydrogen distribution in lattice sites and trap sites near a blunting crack tip under small-scale yielding conditions. The hydrogen transport model of Sofronis and McMeeking (1989) was used. A modification of the hydrogen transport model is proposed which provides a correct hydrogen balance. This was demonstrated in Section 3 in an insulated, uniformly-stressed body. The model is modified by including a (plastic) strain rate factor. It can be concluded that:

(1) when the strain rate factor is not included in the hydrogen transport model, hydrogen is created;
(2) the effect of the strain rate is to reduce the hydrogen concentration in lattice sites due to the filling of trap sites. When the strain rate is relatively low the hydrogen distribution is equal to the steady-state hydrogen distribution. When the strain rate is relatively high the lattice sites can be almost depleted of hydrogen;
(3) the hydrogen concentration in lattice sites near the crack tip is higher in a body with an insulated crack surface than in a body with the hydrogen concentration prescribed on the crack surface.

The modified hydrogen transport model predicts that the hydrogen concentration in lattice sites will be strongly dependent on the strain rate, while the hydrogen concentration in trap sites is not affected. Assuming that the hydrogen in strong trap sites does not contribute to the embrittlement mechanism, the modified hydrogen transport model provides greater insight into the strain rate dependence of hydrogen embrittlement as observed in tensile tests.

Appendix

Variational form of the hydrogen transport equation

Consider a body with volume V bounded by a surface S which consists of a part S_C where the hydrogen concentration is prescribed C_b and a part S_ϕ where the flux through the surface is prescribed by a value ϕ such that

$$\mathbf{J}\cdot\mathbf{n} = \phi. \tag{A1}$$

The parts of the surface S are such that: $S = S_C \bigcup S_\phi$. Multiplying (15) by an arbitrary function C which is differentiable and integrating over the volume of the body gives

$$\int_V C\left\{D^*\frac{\partial C_L}{\partial t}-\nabla\cdot(D_L\nabla C_L)+\nabla\cdot\left(\frac{D_L C_L \bar{V}_H}{RT}\nabla\sigma_h\right)+\theta_T\frac{dN_T}{d\varepsilon_p}\frac{\partial\varepsilon_p}{\partial t}\right\}dV=0, \quad \text{(A2)}$$

where D^* is

$$D^*=\frac{C_L+C_T(1-\theta_T)}{C_L}.$$

However

$$C\nabla\cdot(D_L\nabla C_L)=\nabla\cdot(CD_L\nabla C_L)-\nabla C\cdot(D_L\nabla C_L) \quad \text{(A3)}$$

and

$$C\nabla\cdot\left(\frac{D_L C_L \bar{V}_H}{RT}\nabla\sigma_h\right)=\nabla\cdot\left(C\frac{D_L C_L \bar{V}_H}{RT}\nabla\sigma_h\right)-\nabla C\cdot\frac{D_L C_L \bar{V}_H}{RT}\nabla\sigma_h. \quad \text{(A4)}$$

Hence (A.20 becomes

$$\int_V\left\{CD^*\frac{\partial C_L}{\partial t}-\nabla\cdot(CD_L\nabla C_L)+\nabla C\cdot(D_L\nabla C_L)+\nabla\cdot\left(C\frac{D_L C_L \bar{V}_H}{RT}\nabla\sigma_h\right)\right.$$
$$\left.-\nabla C\cdot\left(\frac{D_L C_L \bar{V}_H}{RT}\nabla\sigma_h\right)+C\theta_T\frac{dN_T}{d\varepsilon_p}\frac{\partial\varepsilon_p}{\partial t}\right\}dV=0. \quad \text{(A5)}$$

Applying the divergence theorem to the second and fourth integral, we find

$$\int_V\left\{CD^*\frac{\partial C_L}{\partial t}+\nabla C\cdot(D_L\nabla C_L)\cdot\frac{D_L C_L \bar{V}_H}{RT}\nabla\sigma_h+C\theta_T\frac{dN_T}{d\varepsilon_p}\frac{\partial\varepsilon_p}{\partial t}\right\}dV$$
$$+\int_S\left(-CD_L\nabla C_L+C\frac{D_L C_L \bar{V}_H}{RT}\nabla\sigma_h\right)\cdot\mathbf{n}\,dS=0. \quad \text{(A6)}$$

We may consider C to be an admissible, arbitrary variation of δC_L of C_L. Since the concentration is fixed on S_C,

$$\delta C=0 \quad \text{on } S_C. \quad \text{(A7)}$$

Substitution of (A.1) and (A.7) in (A.6) gives

$$\int_V\left\{\delta C_L D^*\frac{\partial C_L}{\partial t}+\nabla\delta C_L D_L\nabla C_L-\nabla C\cdot\frac{D_L C_L \bar{V}_H}{RT}\nabla\sigma_h\right.$$
$$\left.+\delta C_L\theta_T\frac{dN_T}{d\varepsilon_p}\frac{\partial\varepsilon_p}{\partial t}\right\}dV+\int_{S_\phi}\delta C_L\phi\,dS=0. \quad \text{(A8)}$$

Finite element form of the hydrogen transport equation

For the finite element formulation we define the interpolation matrix $[A]$, which transforms nodal point variables to local element variables, for example for the hydrogen concentration

$$C_L = [A]\,[C_L], \tag{A12a}$$

where $[C_L]$ is the vector of nodal point concentrations. Matrix $[A]$ is assumed to be time-independent, in which case we can also write

$$\frac{\partial C_L}{\partial t} = [A]\,[\dot{C}_L]. \tag{A12b}$$

Gradients are related to the nodal point values by the gradient matrix $[B]$. For the gradient of the concentration

$$\nabla C_L = [B]\,[C_L] \tag{A12c}$$

and similarly for the hydrostatic stress

$$\nabla \sigma_h = [B]\,[\sigma_h]. \tag{A12d}$$

Using (A12a–d), (A8) can be written in matrix form:

$$\int_V \Bigg\{ [\delta C_L]^T [A]^T D^* [A]\,[\dot{C}_L] + [\delta C_L]^T [B]^T D_L [B]\,[C_L] - [\delta C_L]^T [B]^T \frac{D_L \bar{V}_H}{RT} [B]\,[\sigma_h]\,[A]\,[C_L] + [\delta C_L]^T [A]^T \theta_T \frac{dN_T}{d\varepsilon_p} \frac{\partial \varepsilon_p}{\partial t} \Bigg\} dV + \int_{S_\phi} [\delta C_L]^T [A]^T \phi \, dS = 0. \tag{A13}$$

Since this equation must hold for any admissible variation $[\delta C_L]$, it can be written as

$$\int_V \Bigg\{ [A]^T D^* [A]\,[\dot{C}_L] + [B]^T D_L [B]\,[C_L] - [B]^T \frac{D_L \bar{V}_H}{RT} [B]\,[\sigma_h]\,[A]\,[C_L] + [A]^T \theta_T \frac{dN_T}{d\varepsilon_p} \frac{\partial \varepsilon_p}{\partial t} \Bigg\} dV + \int_{S_\phi} [A]^T \phi \, dS = 0 \tag{A14}$$

or

$$[M]\,[\dot{C}_L] + [K]\,[C_L] = [F], \tag{A15}$$

where $[M]$ is the concentration capacity matrix, given by

$$[M] = \int_V [A]^T D^* [A]\, dV$$

and $[K]$ is the diffusivity matrix $[K] = [K_1] + [K_2]$ given by

$$[K_1] = \int_V [B]^T D_L [B]\, dV$$

and

$$[K_2] = -\int_V [B]^{\mathrm{T}} \frac{D_{\mathrm{L}} \bar{V}_{\mathrm{H}}}{RT} [B]\,[\sigma_{\mathrm{h}}]\,[A]\,\mathrm{d}V$$

and $[F] = [F_1] + [F_2]$ given by

$$[F_1] = -\sum_{\text{elements}} \int_{S_\phi} [A]^{\mathrm{T}} \phi\,\mathrm{d}S$$

and

$$[F_2] = -\int_V [A]^{\mathrm{T}} \theta_{\mathrm{T}} \frac{\mathrm{d}N_{\mathrm{T}}}{\mathrm{d}\varepsilon_{\mathrm{p}}} \frac{\partial \varepsilon_{\mathrm{p}}}{\partial t} \mathrm{d}V.$$

Note that $[M]$, $[K]$ and $[F]$ have, respectively, the characteristics of the mass matrix, the stiffness matrix and the force vector in dynamic stress analysis. Skipping the term $[F_2]$ in (A15) leads to the equation used by Sofronis and McMeeking (1989). Obviously, (A15) is non-linear since $[M]$ depends on the hydrogen concentration in lattice sites and trap sites through the effective diffusion constant D^*. For convenience the left-hand side of (A15) is made symmetrical by putting the term $[K_2]\,[C_{\mathrm{L}}]$ on the right-hand side:

$$[M]\,[\dot{C}_{\mathrm{L}}] + [K_1]\,[C_{\mathrm{L}}] = [F_1] + [F_2] - [K_2]\,[C_{\mathrm{L}}]. \tag{A16}$$

A linear backward difference scheme was used for the discretization of the time variable. A simple estimate of the matrices [M], [K_2], [F_1], and [F_2] at $t+\Delta t$ can be made from the previous step, taking

$$[M]_{t+\Delta t} = [M]_t, \quad [K_2]_{t+\Delta t} = [K_2]_t, \quad [F_1]_{t+\Delta t} = [F_1]_t, \quad \text{and} \quad [F_2]_{t+\Delta t} = [F_2]_t. \tag{A17}$$

Writing the derivatives of the nodal hydrogen concentration as

$$[\dot{C}_{\mathrm{L}}] \approx \frac{1}{\Delta t}([C_{\mathrm{L}}]_{t+\Delta t} - [C_{\mathrm{L}}]_t) \tag{A18}$$

and substitution in (A15) using (A17), results in

$$\left(\frac{1}{\Delta t}[M]_t + [K_1]\right)[C_{\mathrm{L}}]_{t+\Delta t} = \left(\frac{1}{\Delta t}[M]_t - [K_2]_t\right)[C_{\mathrm{L}}]_t + [F_1]_t + [F_2]_t. \tag{A19}$$

This finite element equation is implemented in the MARC finite element program (1990). The hydrostatic stress at the nodes is determined as follows: first, the hydrostatic stress is determined at the Gauss integration points of the finite element as the average of the three normal stresses, $\sigma_{\mathrm{h}} = \frac{1}{3}\Sigma_{i=1}^{3}\,\sigma_{ii}$. Next the average of the hydrostatic stresses in the element is taken, which is used together with the hydrostatic stress at the integration points for linear extrapolation to the nodes. The hydrostatic stress in a node is then the weighted average of the hydrostatic stresses for all elements which are connected to that node, with the element volumes acting as the weighted factors.

References

Cialone, H., Asaro, R.J., 1981. Hydrogen assisted fracture of spheroidized plain carbon steels. Metall. Trans. A 12, 1373–1387.

Gao, H., Cao, W., Fang, C., Rios, E.R. De Los, 1994. Analysis of crack tip hydrogen distribution under I/II mixed mode loads. Fatigue Fract. Eng. Mater. Struct. 17, 1213–1220.

Garber, R., Bernstein, I.M., Thompson, A.W., 1981. Hydrogen assisted ductile fracture of spheroidized carbon steels. Metall. Trans. A 12, 225–234.

Hirth, J.P., 1980. Effects of hydrogen on the properties of iron and steel. Metall. Trans. A 11, 861–890.

Johnson, H.H., Lin, R.W., 1981. Hydrogen deuterium trapping in iron. Hydrogen Effects in Metal, Ed. I.M. Bernstein, A.W. Thompson, pp. 3–23. Metallurgical Society of AIME, New York.

Kiuchi, K., McLellan, E.B., 1983. The solubility and diffusivity of hydrogen in well-annealed and deformed iron. Acta Metall. 31, 961–984.

Krom, A.H.M., 1998. Numerical modelling of hydrogen transport in steel. Ph.D. thesis, Delft University of Technology, The Netherlands.

Kumnick, A.J., Johnson, H.H., 1980. Deep trapping states for hydrogen in deformed iron. Acta Metall. 28, 33–39.

Maier, H.J., Popp, W., Kaesche, H., 1995. Effects of hydrogen on ductile fracture of a spheroidized low alloy steel. Mater. Sci. Eng. A 191, 17–26.

MARC K6.1, 1990. MARC Analysis Research Corporation, Palo Alto, U.S.A.

Smithells Metals Reference Book, 1992. Ed. E.A. Brandis, G.B. Brooks, 7th edn. Buttersworths, London.

Oriani, R.A., 1970. The diffusion and trapping of hydrogen in steel. Acta Metall. 18, 147–157.

Sofronis, P., McMeeking, R.M., 1989. Numerical analysis of hydrogen transport near a blunting crack tip. J. Mech. Phys. Solids 37, 317–350.

Sun, S., Shiozawa, K., Gu, J., Chen, N., 1995. Investigation of deformation field and hydrogen partition around crack tip in fcc single crystal. Metall. Mat. Trans. 26A, 731–739.

Toribio, J., Valiente, A., Cortes, R., Caballero, L., 1995. Modelling hydrogen embrittlement in 316L austenitic stainless steel for the first wall of the Next European Torus. Fusion Eng. Des. 29, 442–447.

Tracey, D.M., 1976. Finite element solutions for crack-tip behavior in small-scale yielding. J. Eng. Mater. Tech. 98, 146–151.

Turnbull, A., 1993. Modelling of environmental assisted cracking. Corrosion Science 34, 921–960.